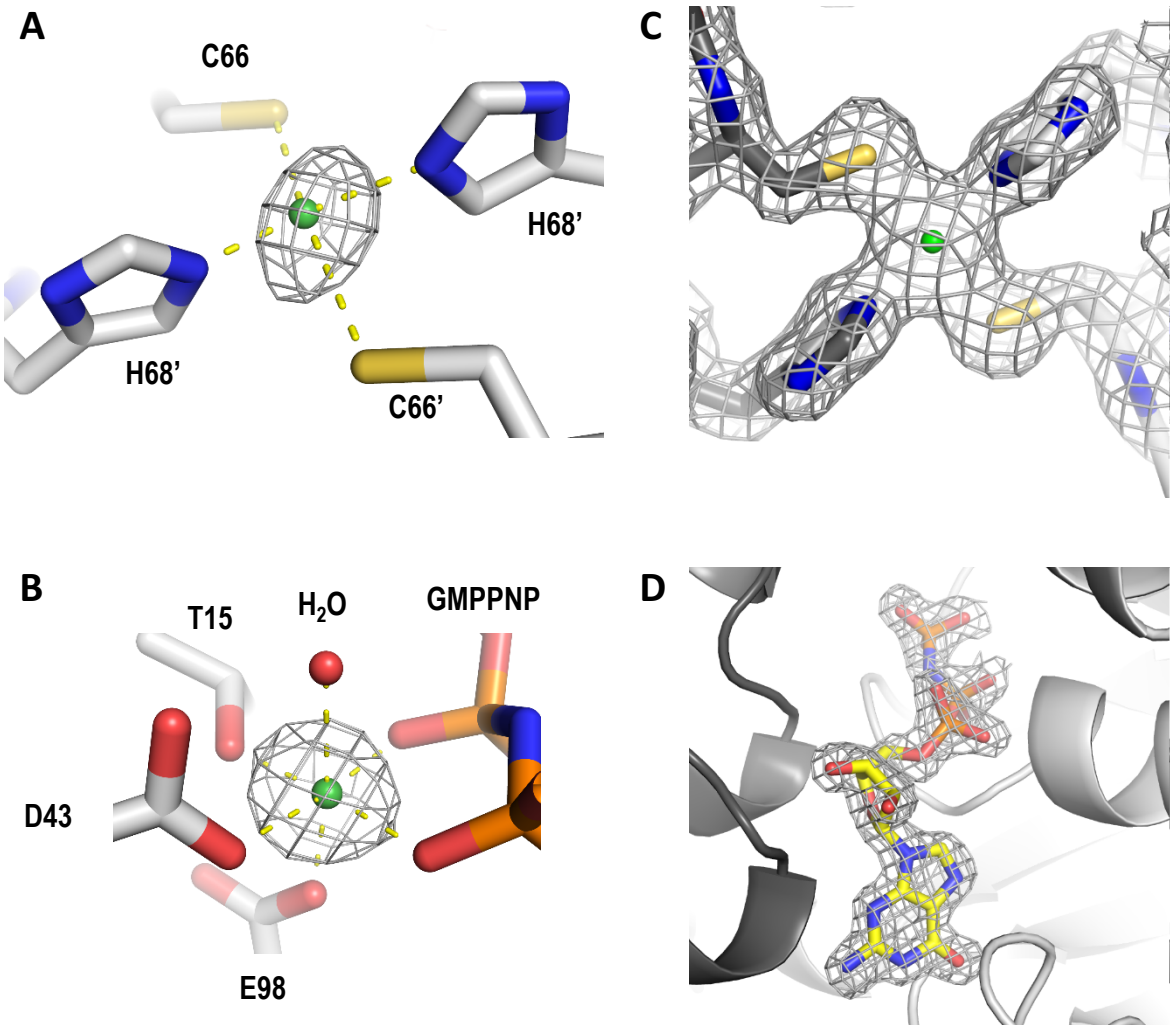

Figure S1. Bound nickel ion identified by anomalous difference map and electron density maps of selected regions of Ni/GMPPNP-bound *Kp*UreG.

In **(A) & (B)**, anomalous difference electron density map, contoured at 7σ, was generated by PHENIX.REFINE using diffraction data collected at the nickel peak wavelength (SI Appendix, Table S2). **(A)** A nickel ion, coordinated in a square-planar geometry by Cys66 and His68 of the CPH motif, is located at the dimer interface of the Ni/GMPPNP-bound *Kp*UreG dimer. Residues from the opposite protomer are indicated by apostrophes. **(B)** A nickel ion was found to occupy the magnesium binding site in the nucleotide binding pocket of UreG, coordinated in an octahedral geometry by Thr15 (G1 motif), Asp43 (G2 motif), Glu98 (G3 motif), β/γ phosphate groups of GMPPNP, and a water. It is noted that the conserved residue Glu98 of the G3 motif is responsible for binding an active site magnesium ion in the G3E family of GTPases (1). Two protomers of *Kp*UreG are colored in light and dark grey. **(C)** 2Fo-Fc electron density map contoured at 1.5σ showing the bound nickel at the dimeric interface. **(D)** Fo-Fc electron density map (before the GMPPNP was modeled) contoured at 3.0σ.

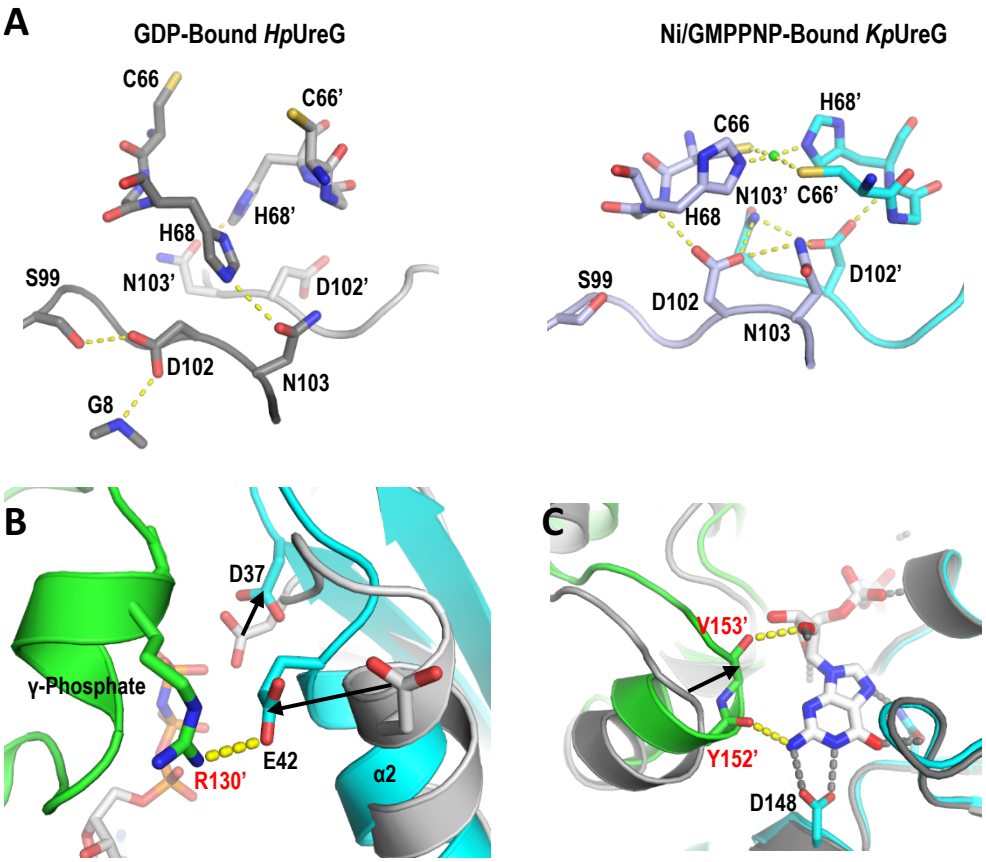

Figure S2. Structural comparison of the GDP-bound *Hp*UreG and Ni/GMPPNP-bound *Kp*UreG

(A) Reorganization of hydrogen bonding network in the metal binding motif. In the GDP-bound state, His68 forms hydrogen bond with the conserved Asn103 (G3) and is pointing away from the nickel binding site. In the GTP-bound state, this hydrogen bond is broken, and Asp102 flips up to form hydrogen bonds with His68, Asn103 and Asn103' from the opposite protomer. Residues from the opposite protomer are indicated by apostrophes. **(B)** Charge-charge repulsion between the γ-phosphate group and Asp37 elicits conformational changes that induce helix-2 to tilt towards the nucleotide-binding site and bring Glu42 to form a salt-bridge with Arg130 of the opposite protomer. **(C)** The opposite protomer of UreG (green) undergoes a rigid-body movement towards the bound GMPPNP, forming two extra hydrogen bonds (yellow dotted lines) as indicated.

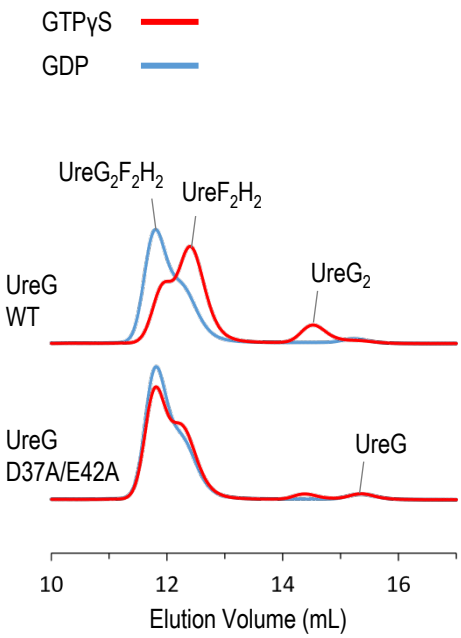

Figure S3. Dissociation of UreG from the $UreG_2F_2H_2$ complex in the presence of GTPγS was greatly reduced in the *H. pylori* UreG D37A/E42A double mutant.

Protein samples of 15 μM of $UreG_2F_2H_2$ complex (wild-type or mutant) were mixed with 45 μM nickel ion and 300 μM GTPγS (red lines) or GDP (cyan lines), and were analyzed by SEC/SLS. In the presence of GTPγS, wild-type UreG dissociated from $UreG_2F_2H_2$ to form a UreG dimer, while the dissociation was greatly reduced in the UreG D37A/E42A mutant.

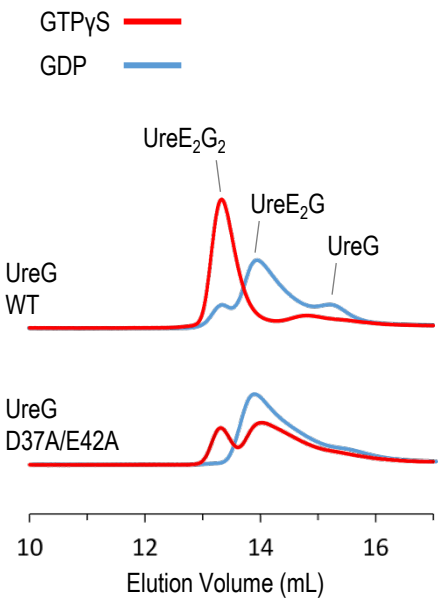

Figure S4. GTP-dependent formation of the $UreE_2G_2$ complex was greatly reduced in *H. pylori* UreG D37A/E42A mutant.

Protein samples of 30 μM UreG (wild type or mutant) were mixed with 30 μM UreE, 45 μM nickel ion and 300 μM GTPγS (red lines) or GDP (cyan lines), and were analyzed by SEC/SLS. In the presence of GTPγS, wild type UreG interacted with UreE to form a $UreE_2G_2$ complex. The ability to form the $UreE_2G_2$ complex in the presence of GTPγS was greatly reduced in the D37A/E42A mutant.

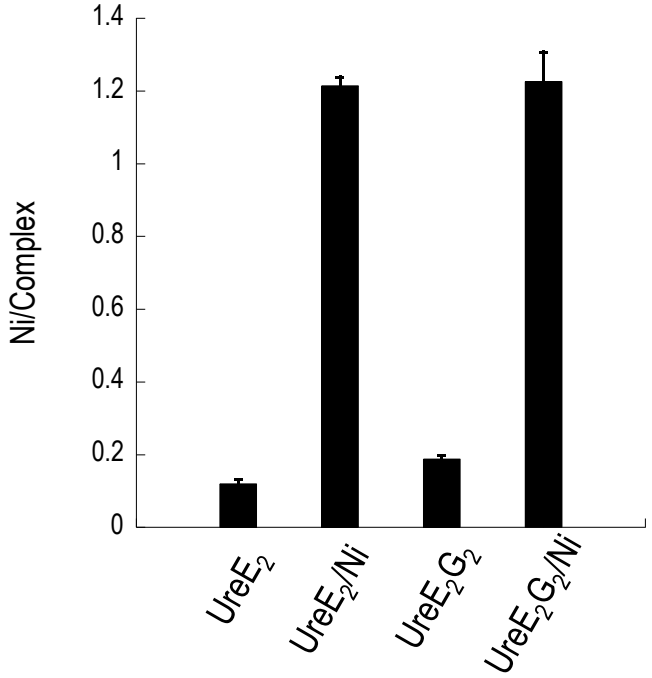

Figure S5. Preparation of the nickel-charged UreE dimer ($UreE_2$/Ni) and the nickel-charged $UreE_2G_2$ complex ($UreE_2G_2$/Ni).

To prepare $UreE_2$/Ni, 200 μM purified $UreE_2$ sample was mixed with 1 mM $NiSO_4$. Excess nickel was removed by a HiTrap Desalting column (GE Healthcare). To prepare the $UreE_2G_2$/Ni complex, equal molar ratio (~100 μM) of nickel-charged UreE dimer and UreG was mixed in the presence of 2 mM $MgSO_4$ and 1 mM GTP, followed by gel filtration chromatography using a Superdex 200 Increase 10/300 gel filtration column (GE Healthcare). To prepare the $UreE_2G_2$ complex without the bound nickel ($UreE_2G_2$), apo-$UreE_2$ and UreG were mixed instead. The nickel content in $UreE_2$, $UreE_2$/Ni, $UreE_2G_2$, $UreE_2G_2$/Ni complexes prepared were determined by atomic absorption spectroscopy, which confirmed that one nickel ion was bound per $UreE_2$/Ni or $UreE_2G_2$/Ni. The protein complexes were also found to be of correct molecular weight by SEC/SLS (SI Appendix, Figure S8).

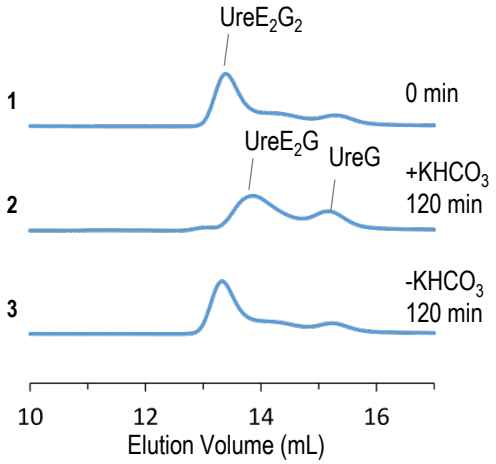

Figure S6. Dissociation of $UreE_2G_2$ to $UreE_2G$ upon GTP Hydrolysis.

15 μM $UreE_2G_2$/Ni complex (injection 1) in 1 mM GTP, 0.2 mM TCEP, 100 mM NaCl, 20 mM HEPES, pH 7.2 was incubated with (injection 2) or without (injection 3) 10 mM $KHCO_3$ at 37 ˚C for 120 min. Protein samples were then analyzed by SEC/SLS. Our results showed that the $UreE_2G_2$ complex dissociated into $UreE_2G$ and a monomeric UreG (injection 2) upon activation of GTP hydrolysis by $KHCO_3$.

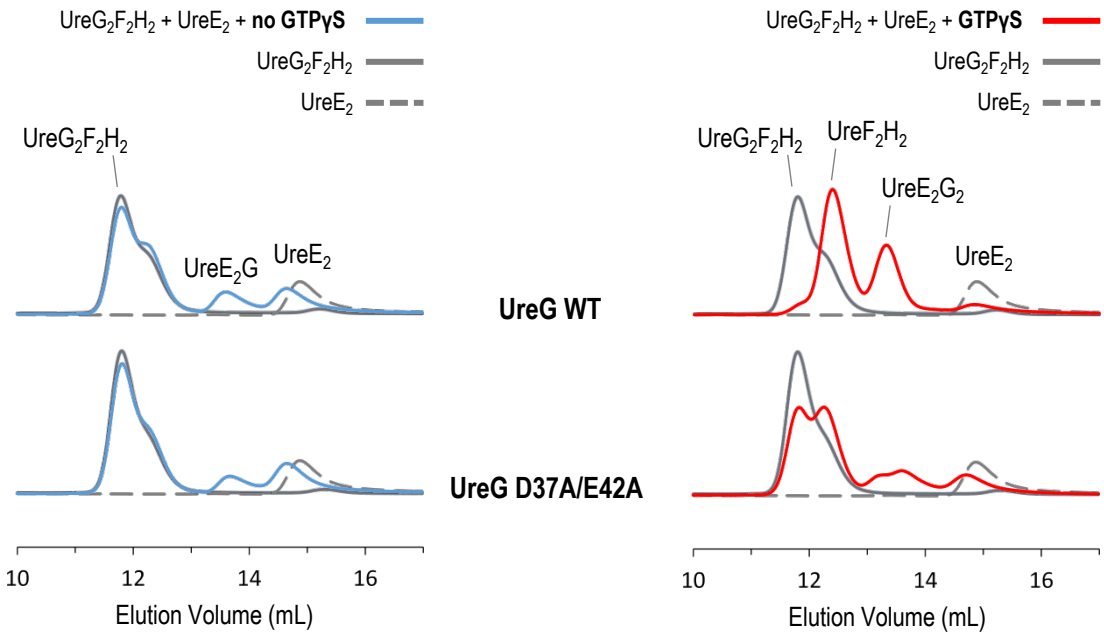

Figure S7. The switching of UreG from the $UreG_2F_2H_2$ complex to the $UreE_2G_2$ complex is dependent on GTP but not on nickel.

15 μM $UreG_2F_2H_2$ complex (grey solid lines) and 15 μM apo-UreE dimer (grey dotted lines) was added to 2 mM $MgSO_4$, 0.2 mM TCEP, 100 mM NaCl, 20 mM HEPES, pH 7.2 buffer with (red lines) or without (cyan lines) 300 μM GTPγS. The protein samples were analyzed by SEC/SLS. In the absence of GTPγS (left panel), only small amount of UreG dissociated from the $UreG_2F_2H_2$ complex to form the $UreE_2G$ complex. In the presence of GTPγS (right panel), wild-type UreG completely dissociated from the $UreG_2F_2H_2$ complex to form the $UreE_2G_2$ complex with the apo-UreE dimer. For the UreG D37A/E42A mutant, the GTP-dependent swapping of protein binding partners was greatly abolished.

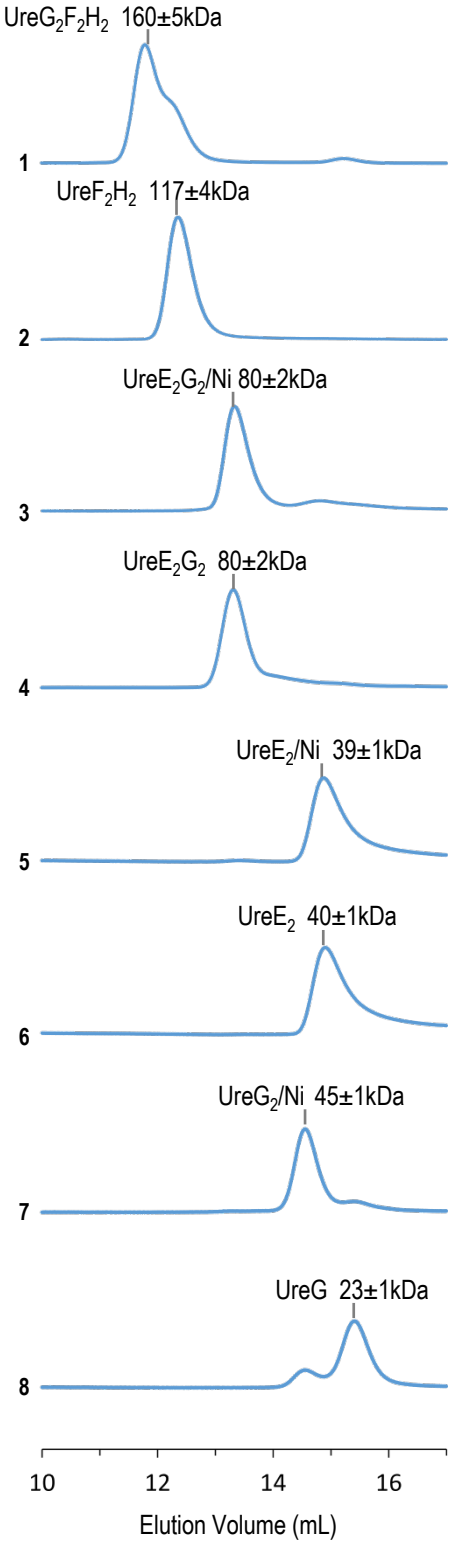

Protein/ Complex	Expected MW
$UreG_2F_2H_2$	161
$UreF_2H_2$	117
$UreE_2G_2$	83
$UreE_2$	39
$UreG_2$	44
UreG	22

Figure S8. Size-exclusion-chromatography/static-light-scattering (SEC/SLS) analyses of urease accessory proteins and their complexes.

Protein samples of urease accessory proteins and their complexes were prepared and analyzed by SEC/SLS using a Superdex 200 Increase 10/300 column as described in the Materials and Methods. The elution volumes of (1) $UreG_2F_2H_2$, (2) $UreF_2H_2$, (3) nickel-charged $UreE_2G_2$, (4) apo-$UreE_2G_2$, (5) nickel-charged UreE dimer, (6) apo-UreE dimer, (7) nickel-charged UreG dimer, and (8) UreG monomer, were 11.8, 12.4, 13.3, 13.3, 14.9, 14.9, 14.5, and 15.5 mL, respectively. The molecular weights estimated by static-light-scattering were indicated at the elution peak, and they agreed well with the expected molecular weights.

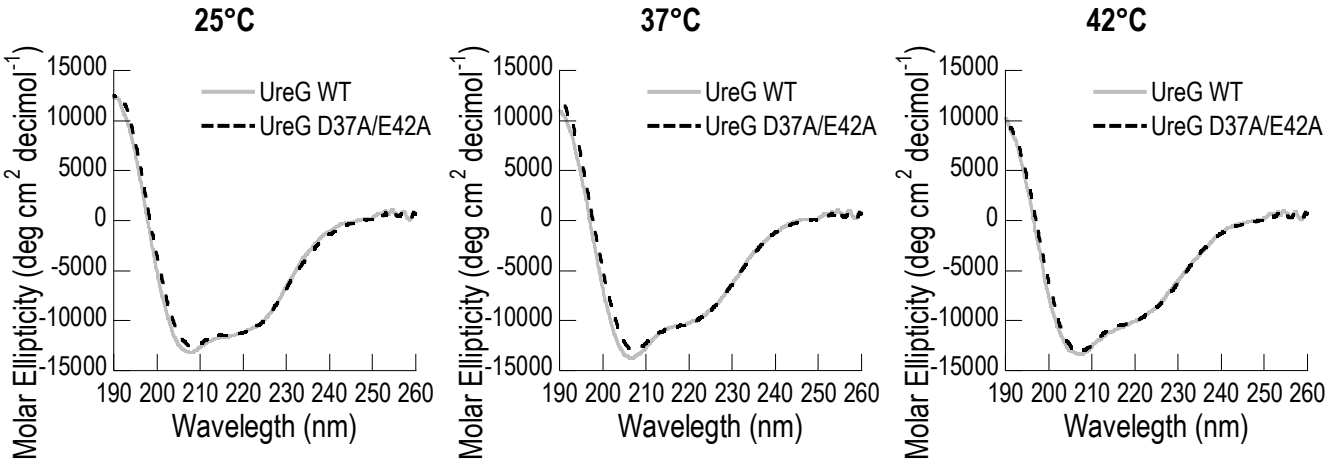

Figure S9. Circular dichroism spectra of wild-type (solid lines) and D37A/E42A (dotted lines) *H. pylori* UreG.

The spectra collected were similar at 25˚C, 37˚C and 42˚C, suggesting that both wild-type and the mutant were folded and stable at these temperatures.

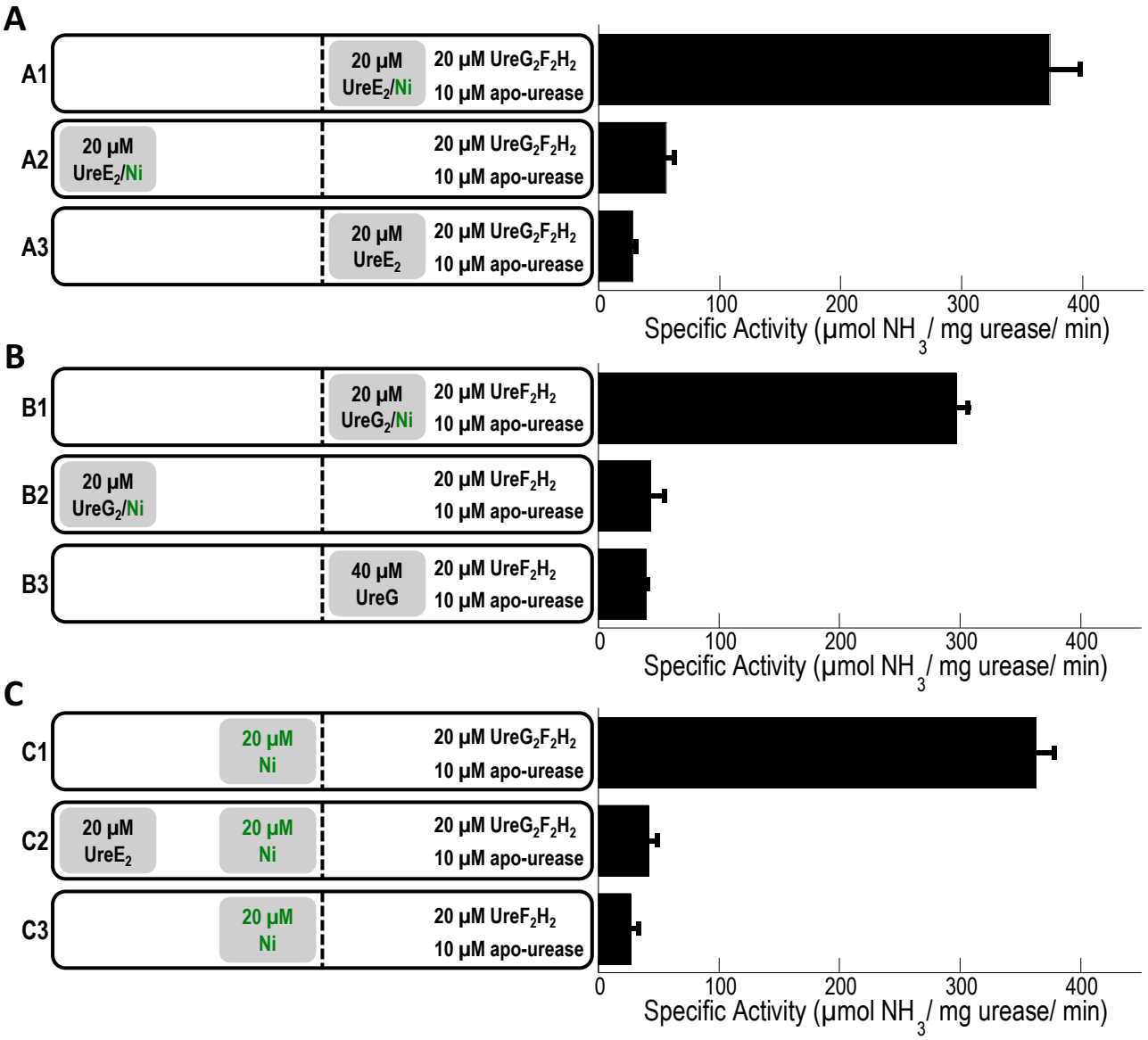

Figure S10. Protein-protein interactions are essential for *in-vitro* urease activation.

To test if protein-protein interactions are essential to the urease activation, urease accessory proteins ($UreE_2$/Ni, $UreG_2$/Ni, apo-$UreE_2$, apo-UreG, $UreG_2F_2H_2$, $UreF_2H_2$) and apo-urease were added to either side of a dialysis membrane (dotted lines) in a two-chamber dialyzer (solid lines). The concentrations and the location of the proteins added are indicated schematically in the left panel. The buffer in both chambers contained 20 mM HEPES pH 7.5, 200 mM NaCl, 1 mM TCEP, 2 mM $MgSO_4$ and 300 μM GTP. The dialysis membrane allows diffusion of nickel ions but prevents direct protein-protein interactions across the membrane. After equilibration at 4 ˚C for 16 hr, 10 mM $KHCO_3$ was added to both chambers to activate the GTP hydrolysis required for urease activation. **(A) & (B)**. Urease was activated only when $UreE_2$/Ni or $UreG_2$/Ni were added to the right chamber where other urease accessory proteins and apo-urease were located (A1 and B1). On the other hand, urease activation was greatly abolished when $UreE_2$/Ni or $UreG_2$/Ni were added in the left chamber and were separated from apo-urease and other urease accessory proteins by the dialysis membrane (A2 and B2). Urease activation was nickel dependent as addition of apo-$UreE_2$ (A3) or apo-UreG (B3) failed to activate urease. **(C)** We added 20 μM $NiSO_4$ to the left chamber as indicated, and showed that free nickel ions, if presence, could diffuse across the dialysis membrane and activate urease in the right chamber with $UreG_2F_2H_2$ (C1), but not with $UreF_2H_2$ (C3). However, activation of urease was inhibited by addition of apo-$UreE_2$ (C2) in the left chamber.

Table S1. Data collection and refinement statistics.

Data collection	
Wavelength (Å)	1.54
Space group	I2
Cell dimensions	
a, b, c (Å)	83.55, 49.32, 129.70
α, β, γ (°)	90.0, 103.17, 90.0
Resolution (Å)	19.43-1.80 (1.84-1.80)
R_{merge}	0.060 (0.462)
$I/\sigma I$	13.1 (2.6)
Completeness (%)	99.7 (99.8)
Redundancy	3.5 (3.4)
Refinement	
Resolution (Å)	19.43 – 1.80
No. reflections	47824 (2812)
R_{work} / R_{free}	0.1563 / 0.1905
No. atoms	
Protein	2982
Ligand/ion	67
Water	488
B-factors (Å^2)	
Protein	21
Ligand/ion	13
Water	33
R.m.s. deviations	
Bond lengths (Å)	0.014
Bond angles (°)	1.315
Ramachandran	
Favored (%)	98
Allowed (%)	2
Outliers (%)	0

*Values in parentheses are for highest-resolution shell.

Table S2. Data collection statistics for nickel anomalous data.

Data collection	Ni-peak
Wavelength (Å)	1.4853
Space group	$P2_1$
Cell dimensions	
a, b, c (Å)	84.06, 49.38, 129.61
α, β, γ (°)	90.0, 102.39, 90.0
Resolution (Å)	30.32-1.80 (1.83-1.80)
R_{merge}	0.042 (0.288)
$I/\sigma I$	29.9 (6.7)
Completeness (%)	99.8 (99.1)
Redundancy	6.4 (6.1)

*Values in parentheses are for highest-resolution shell.

SI Reference

1. Wittinghofer A, Vetter IR (2011) Structure-function relationships of the G domain, a canonical switch motif. *Annu Rev Biochem* 80:943–71.